Supplementary Text

Quality of the electromyographic and nerve cord recordings obtained by wireless telemetry. The recordings obtained with the telemetry system were comparable to those obtained with conventional laboratory equipment, with two minor differences. The first difference was in the electromyographic recordings of flexor activity. With the transmitter, we typically detected activity in the flexors at the time of co-contraction (e.g., Fig. 1 and 3) while conventional recordings show detectable activity before the IJM (Fig. 4 of Fotowat and Gabbiani 2007). The most likely explanation for this difference is the gain of the muscle channels in the telemetry system. Alternatively, it may be due to electrode placement in the current experiments. The second difference concerns the DCMD spikes that we detected by applying a voltage threshold to the received nerve cord recording (Supplementary Figure 7). The DCMD spikes could be reliably detected at most times throughout the trial (Supplementary Figure 7Aa). Around the time of the DCMD peak-firing rate, in 84% of the *jump* trials, we found that the DCMD spikes could not be detected as reliably. The received waveform showed distortions over time intervals in the range 2-10 ms (Supplementary Figure 7Ab). We suspect the main reason for these distortions to be the multi-unit spiking activity of descending neurons, including the DCMD, at a rate that exceeds the sampling rate of the telemetry system. Based on the estimated peak firing rate, and given the short duration of these distortions, we estimate that we might have missed at most 3 consecutive spikes around the timing of the peak firing rate. More specifically in 46% of the trials we could have missed less than 2 DCMD spikes and in the other 38% we could have missed between 2-3 spikes. Such distortions were never observed in the no jump trials (Supplementary Figure 7B). In the

trial depicted in Figure 1 and S7, we e.g., we could have missed at most 3.38 DCMD spikes (peak firing rate=338 spk/s, duration of distortions = 10 ms). Adding 3 DCMD spikes to the raster uniformly over 10 ms (red spikes) increased the peak firing rate to 387 spk/s (red instantaneous firing rate trace). For l/|v|=80 ms, there were four trials in which 3 spikes could have been missing. Adding those spikes on average increased the peak firing rate by 11.3% (SD=1.4%, n=4, n_L=1), however this effect on the firing rate was not significant (p_{KWT}=0.38). Adding those spikes shifted the average peak time by 6.4 ms (SD=6.1), which was not significant either (p_{KWT}=0.77). Moreover, we found that the peak rate and number of DCMD spikes after the onset of co-contraction were significantly higher in jump trials and therefore, this possible (and non-significant) underestimation does not affect any of our conclusions.

Correlation between sensory and motor attributes during behavior. Besides the correlation between the number of DCMD spikes counted from co-contraction onset and the number of extensor spikes reported in the main text, we found a small but significant correlation between the number of extensor spikes and the peak DCMD firing rate (ρ = 0.3, p = 0.01). In addition, there was a high correlation between the time of start of co-contraction and the number of extensor spikes ($\rho_{extensor}$ = 0.64, $p < 10^{-9}$). The number of DCMD spikes counted from co-contraction onset was also highly correlated with the time of start of co-contraction (ρ_{DCMD} = 0.75, $p<10^{-9}$). This is expected since the earlier the co-contraction starts, the more DCMD spikes will be generated as the stimulus angular size increases. The number of DCMD spikes was also correlated with the DCMD peak firing

rate ($\rho = 0.57$, $p < 10^{-9}$), which itself was independent of the time of start of co-contraction ($\rho = 0.1$, $p = 0.2$).

Since the number of extensor spikes is correlated with both the number of DCMD spikes and the time of start of co-contraction (which are themselves highly correlated), we used a partial correlation analysis to examine the relationship between the number of extensor spikes and the time of start of co-contraction, controlling for the correlation with the number of DCMD spikes. We found that in fact, controlling for the effect of the number of DCMD spikes, there was no significant correlation between the time of start of co-contraction and the number of extensor spikes ($\rho = 0.2$, $p = 0.1$). On the other hand, controlling for the peak firing rate, the correlation between the number of DCMD and extensor spikes still holds ($\rho = 0.7$, $p = 1.14 \times 10^{-9}$), whereas controlling for the number of DCMD spikes, there remained no correlation between peak firing rate and the number of extensor spikes ($\rho = -0.2$, $p = 0.1$). These results further strengthen the argument presented in the main text that the number of DCMD spikes chiefly determines the number of extensor spikes, once co-contraction has started.

Classification of jump vs. no jump trials based on sensory-motor attributes. As illustrated in Figure 5C, the number of DCMD spikes from co-contraction onset (1) and the timing of start of co-contraction (2) were the best predictors of the trial outcome, ($p_{KWT} < 0.0005$). The next best predictor was the number of extensor spikes (3). As expected, an increase in the number of DCMD spikes following co-contraction onset implies a decrease of the mean Inter-Spike Interval (ISI) during that single trial. In addition, the

standard deviation (SD) of the same ISI sequence decreases as well, since its mean is closer to the DCMD refractory period. Therefore, the mean and SD of the ISI sequences following co-contraction onset were significantly lower in jump trials. The classifiers trained with the SD (4) and mean (5) of the ISI sequences performed similarly. The classifier trained on the DCMD peak firing rate (6) had significantly higher error rates than the one trained on the number of spikes (1). We found that the partial correlation between the number of DCMD and extensor spikes, controlling for the DCMD peak firing rate, was larger for smaller mean ISI values (below the median; $\rho_{high\ ISI} = 0.65$, $p=2.7x10^{-4}$; $\rho_{low\ ISI} = 0.78$, $p=2.8x10^{-6}$). This result suggests that the smaller the mean and the SD of the DCMD ISI sequence, the more efficiently DCMD spikes are summated by the inter- and motor neurons that drive the extensor muscle. Moreover, the performance of the classifier improved when it was trained on the number of extensor spikes and the SD of the ISI sequence, or the number of extensor spikes and the mean of the ISI sequence (7 and 8). Although the mean and SD were highly correlated ($\rho = 0.9$ $p< 10^{-9}$), this correlation was smaller for smaller mean ISI values (below the median; $\rho = 0.57$, $p=0.001$). In order to determine which one of the two attributes is a better predictor of the trial outcome, we trained two classifiers, one with the mean and the other with the SD of the ISI sequence. The training set consisted of half of the data having the smaller ISI values (below the median). We then tested these classifiers with a data set chosen randomly from all the data points. This random selection was carried out 100 times and the error rate of the classifiers was compared. We found that classifiers trained with the SD of the DCMD ISI sequence in single trials did significantly better than the ones

trained on its mean (Supplementary Fig. 3). These results suggest that the regularity of the DCMD spikes contributes to their summation at the motor level.

Figure Legends:

Figure S1: Wireless telemetry system for measuring neural and muscle activity in freely behaving locusts and behavioral setup. **A)** The complete transmitter system consists of the custom designed insect telemetry chip, two battery holders, an external crystal, and an accelerometer (both mounted on the bottom surface of the printed circuit board), and a few resistors and capacitors. **B)** The transmitter system was mounted like a saddle on the back of the locust and secured in place using a mixture of rosin and beeswax. The wires implanted around the nerve cord and the muscles were then soldered to the inputs of the chip via miniature connectors. **C)** Photograph of the chip die (2.57 x 2.48 mm^2). The chip receives as input the accelerometer, neural, and muscle recordings, and amplifies, multiplexes, digitizes, and wirelessly transmits them. **D)** The custom designed receiver, loads the received signal into a PC via the USB port, through which it also gets power (for further details, see Harrison et al., 2010). **E)** Schematics of the behavioral setup (for further details, see Fotowat and Gabbiani, 2007). The looming stimulus was presented from one side, leading to monocular stimulation. **F)** Illustration of the neural recordings carried out and analyzed in this work. All sensory inputs originate from the eye facing the stimulus. The DCMD projects through the contralateral nerve cord to thoracic motor centers, while the DIMD projects through the ipsilateral nerve cord. We could also isolate multi-unit activity (MU) in response to looming in the contralateral nerve cord.

Figure S2: Sensory and motor activity in response to looming and "double looming" stimuli (related to Fig. 4). **A)** During looming in jump trials, the amplitude of the DCMD

peak firing rate was significantly larger than in no jump trials for l/|v|=80 and 120 ms. Kruskal-Wallis test p values and the number of trials is shown on the plots (data from 10 locusts). **B)** Example of nerve cord and muscle responses recorded during the presentation of a 'double loom' stimulus. The stimulus started expanding from an angular size of 2º with l/|v|=40 ms up to an angular size of 45º, after which it started expanding again from an angular size of 30º degrees with l/|v|=120 ms to the final size of 130º. Both the DCMD and the extensor muscle firing rates showed two peaks. The symbol [◁] marks the final angular size of the stimulus.

Figure S3: Comparison between the error rate of a classifier that was trained with the mean and the SD of the DCMD ISI. The training set consisted of half of the data with ISI values smaller than the median ISI. Chance level: 0.5. See Supplementary Text for details (related to Fig. 5).

Figure S4: Relation between a DCMD firing rate threshold, stimulus final angular size, and the occurrence of co-contraction (related to Fig. 6). **A)** Probability Density Function of the angular size for trials with and without co-contraction in experiments where the looming stimulus was stopped at different final angular sizes. The kernel bandwidth is equal to 10º. **B)** The DCMD maximum firing rate was variable for any given final angular size. The symbols [*], and [*] mark the trials with, and without co-contraction, respectively. **C)** Plot of the total number of extensor spikes vs. the DCMD maximum firing rate. The symbols [*], and [*] mark the trials with, and without co-contraction, respectively. The dashed line marks the firing rate threshold for classification obtained from a Fisher linear discriminant analysis based on the maximum DCMD firing rate. This analysis reveals that co-contraction is triggered after the DCMD firing rate reaches a

threshold of 248 spk/s. Thus, the maximal DCMD firing rate was a better predictor of co-contraction onset than final stimulus size (the experimental parameter systematically manipulated in these experiments). In A-C: data from 9 locusts. **D)** Trial where only two spikes were triggered in the extensor muscle. In this example, the co-contraction started 27 ms after the maximum firing rate of 243 spk/s (l/|v|=40 ms; stimulus final size=21º). On average the delay between the maximum DCMD firing rate and the start of co-contraction was of 36 ms (SD: 23), and the value of the maximum DCMD firing rate was 300 spk/s (SD=72). Data from 6 locusts tested with looming stimuli with different final sizes. **E)** Time remaining to collision at the start of co-contraction as a function of the time remaining to collision at a threshold firing rate of 225 spk/s (61 trials with full looming stimulus expansion, l/|v| values pooled; data from 4 locusts). **F)** Firing rate of the fast Extensor Tibiae (FETi) motor neuron as a function of the DCMD firing rate during the presentation of looming stimuli with full stimulus expansion (n_L = 4). Five representative trials are plotted per animal (different shades of the same color), illustrating the initial rising phase of the FETi firing rate, up to 25% of its peak. To quantify the steepness of the DCMD firing rate threshold causing co-contraction, the difference in DCMD firing rate between 5% and 25% of the FETi peak firing rate, $\Delta DCMD = DCMD_{FETi\text{-}25\%} - DCMD_{FETi\text{-}5\%}$, was normalized by the peak DCMD firing rate on a trial by trial basis (bottom right inset). The distribution of the resulting steepness index, $\Delta DCMD/DCMD_{peak}$, is plotted in the top right inset (n_L = 4, n_T = 61). A linear relation between DCMD and FETi firing rates from 0 spk/s to their peaks, corresponds to a steepness index of 0.2 (i.e., a 20% DCMD firing rate change, identical to that of the

FETi). Smaller values indicate a steeper threshold. The mean selectivity index, 0.052 (SD: 0.097), was significantly smaller than 0.2 ($p = 0.66$, t-test).

Figure S5: Comparison of DCMD and DIMD peak firing rates and times (related to Fig. 7). **A)** The DCMD peak firing rate was significantly higher than that of the DIMD only at $l/|v|$=10 ms. Kruskal-Wallis p values for $l/|v|$=10-120 ms are 0.0003, 0.5, 0.6, 0.8, 0.6, 0.8, 0.15, 0.9, and 0.16, respectively. **B)** For $l/|v|$ values larger than 50 ms the timing of the peak firing rates were not significantly different. For $l/|v|$ values smaller than 50 ms the DCMD firing rate peak occurred significantly earlier than that of the DIMD. Kruskal-Wallis p values for $l/|v|$=10-120 ms are $10x10^{-7}$, 0.0006, 0.0009, 0.0002, 0.15, 0.11, 0.06, 0.7, 0.6 respectively. The number of trials is shown on the plot ($n_L = 9$).

Figure S6: Example DCMD recordings before, during, and after its laser ablation, as well as comparison of the activity evoked in the intact nerve cord after sectioning of the other nerve cord and laser ablation of the DCMD at the end of the behavioral experiments (related to Fig. 8). **A)** Intra- and extracellular recordings obtained from the DCMD axon (top and bottom panel respectively). After filling the DCMD with a fluorescent dye for 12 min, a laser beam was directed to the filled axon and shone for 3 min, during which the DCMD response to looming stimuli ceased gradually (**B**, top and bottom panels). Note that other looming-responsive units fire close to the collision time. The symbol [◁] points to the final stimulus angular size. **C)** Looming stimuli were presented to the eye ipsi- and contralateral to the remaining nerve cord and the extracellular activity of the nerve cord was recorded. The largest spikes measured for ipsilateral stimulation (gray) correspond to the DIMD. To detect the multi-unit (MU) activity evoked in response to stimuli presented to the contralateral eye (black) a threshold was applied to the recording

just above baseline. Dashed lines indicate peak MU and DIMD activity. **D)** The timing of the peak multi-unit activity evoked in the contralateral nerve cord was delayed relative to that of the DIMD evoked in response to the stimulation of the ipsilateral eye. Kruskal-Wallis p values and the number of trials are shown on the figure. The inset illustrates how the DIMD (magenta) was activated by ipsilateral stimulation (grey triangle) and the MU activity (yellow) by contralateral stimulation (black triangle). Red scissors indicate sectioned nerve cord and blue arrows photoablation of DCMD (green line).

Figure S7. Reliability of DCMD spike detection from the received wireless telemetry data. **A)** The top panel depicts the same example trial as shown in Figure 1. Two time intervals (a and b) are shown on an expanded time scale in the bottom panels. The DCMD spikes can be reliably detected before and after the start of co-contraction (a). Around the time of the peak DCMD firing rate, the nerve recording showed distortions in jump trials (b). In this example 3.3 DCMD spikes could have been missed due to these distortions (see Supplementary text). Adding 3 spikes to the raster (red spikes) results in 11.4 % increase in the amplitude of the DCMD peak firing rate (red trace on the top panel), and a 7.8 ms shift in its timing. Such distortions around the peak were absent in the no jump trials (**B**, same example trial as in Figure 3).

Movie S1. Example video recording of a trial in which the locust jumped in response to a looming stimulus (l/|v|=80 ms, same trial as shown in Figure 1). The sound of the DCMD and muscle spikes synchronized to the movie frames can be heard as high and low pitch tones, respectively.

Movie S2. Example video recording of a trial in which the locust did not jump in response to a looming stimulus (l/|v|=80 ms, same trial as shown in Figure 3). The sound of the DCMD and muscle spikes synchronized to the movie frames can be heard as high and low pitch tones, respectively.

Supplementary References

Harrison, R., Fotowat, H., Chan, R., Kier, R. J., Leonardo, A., & Gabbiani, F. A wireless neural/EMG telemetry system for freely moving insects. To appear in: Proceedings of the 2010 IEEE International Symposium on Circuits and Systems (ISCAS 2010), Paris, France, 2010.

Figure- S1 (Fotowat et al.)

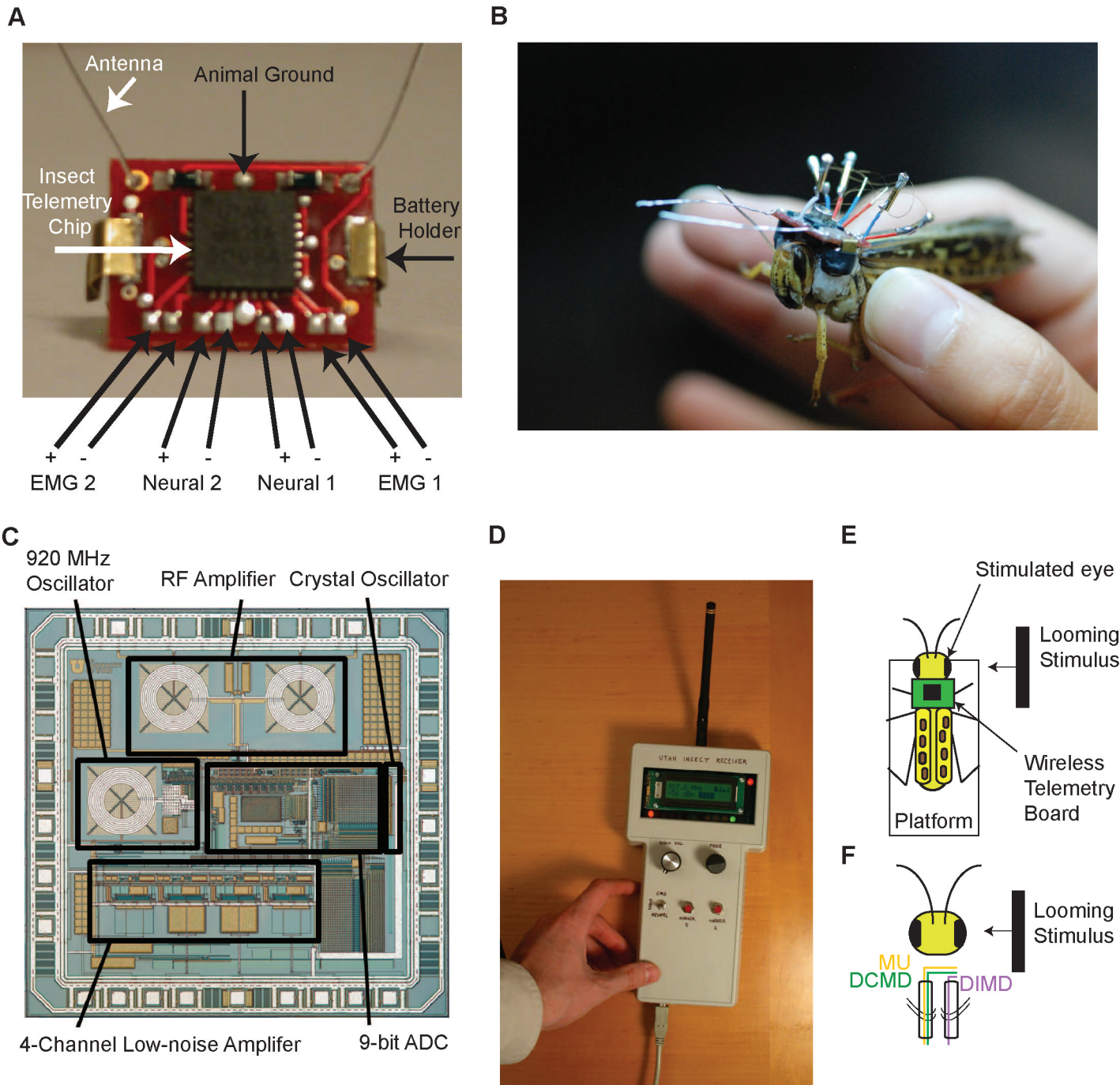

Figure- S2 (Fotowat et al.)

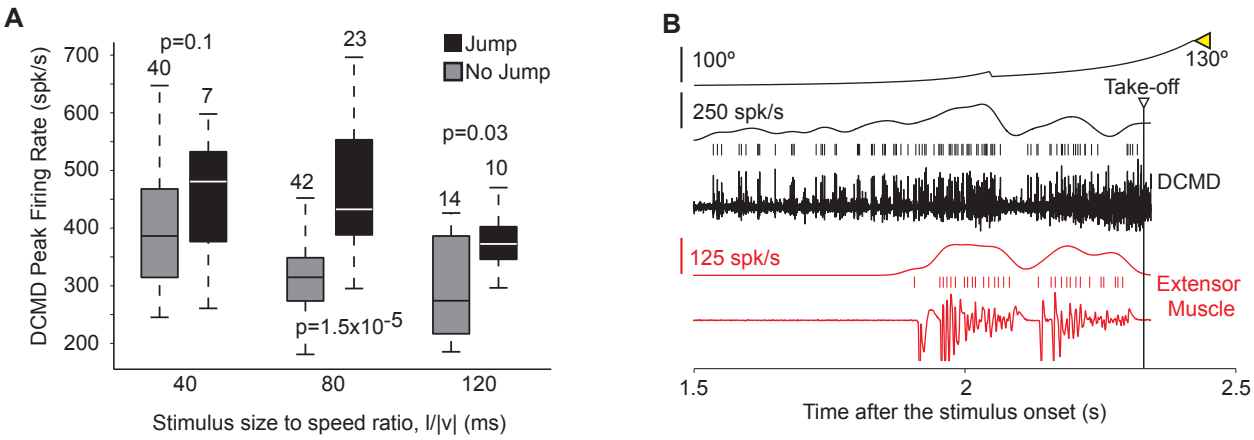

Figure- S3 (Fotowat et al.)

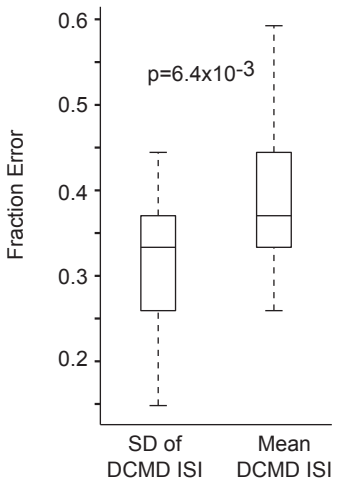

Figure- S4 (Fotowat et al.)

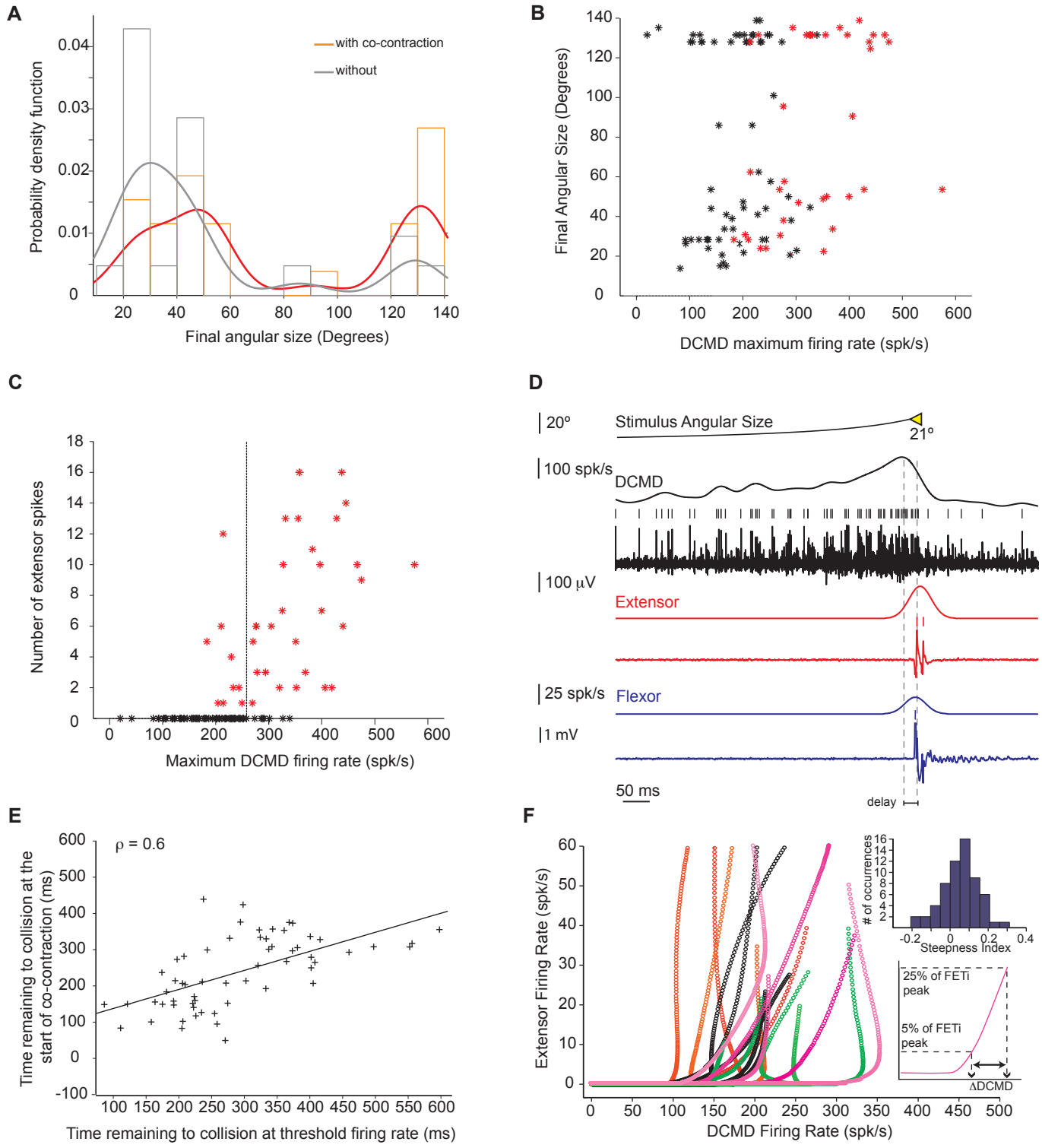

Figure- S5 (Fotowat et al.)

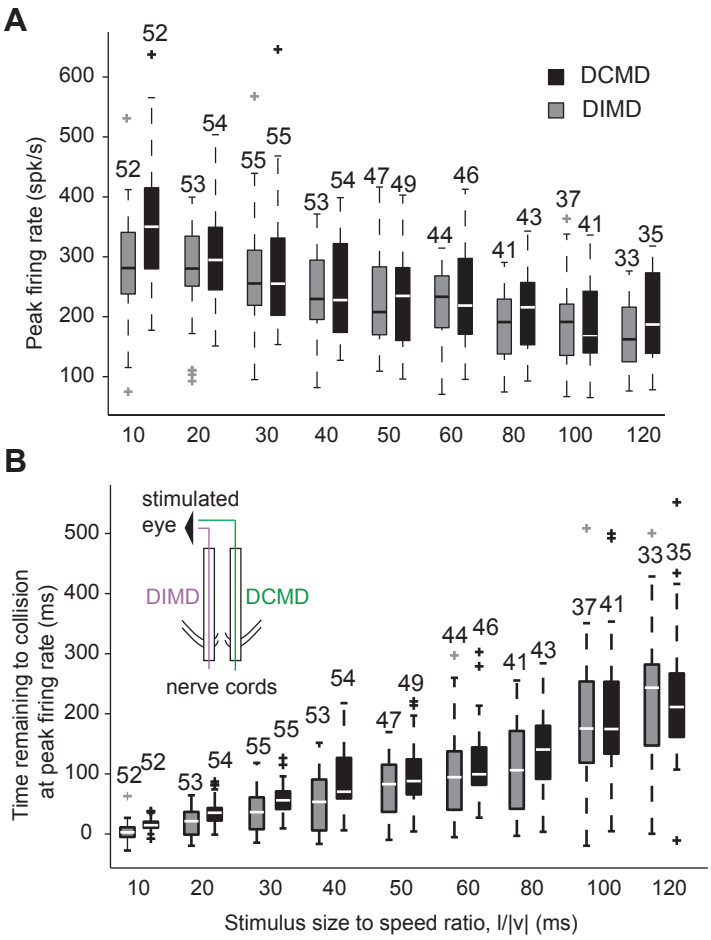

Figure- S6 (Fotowat et al.)

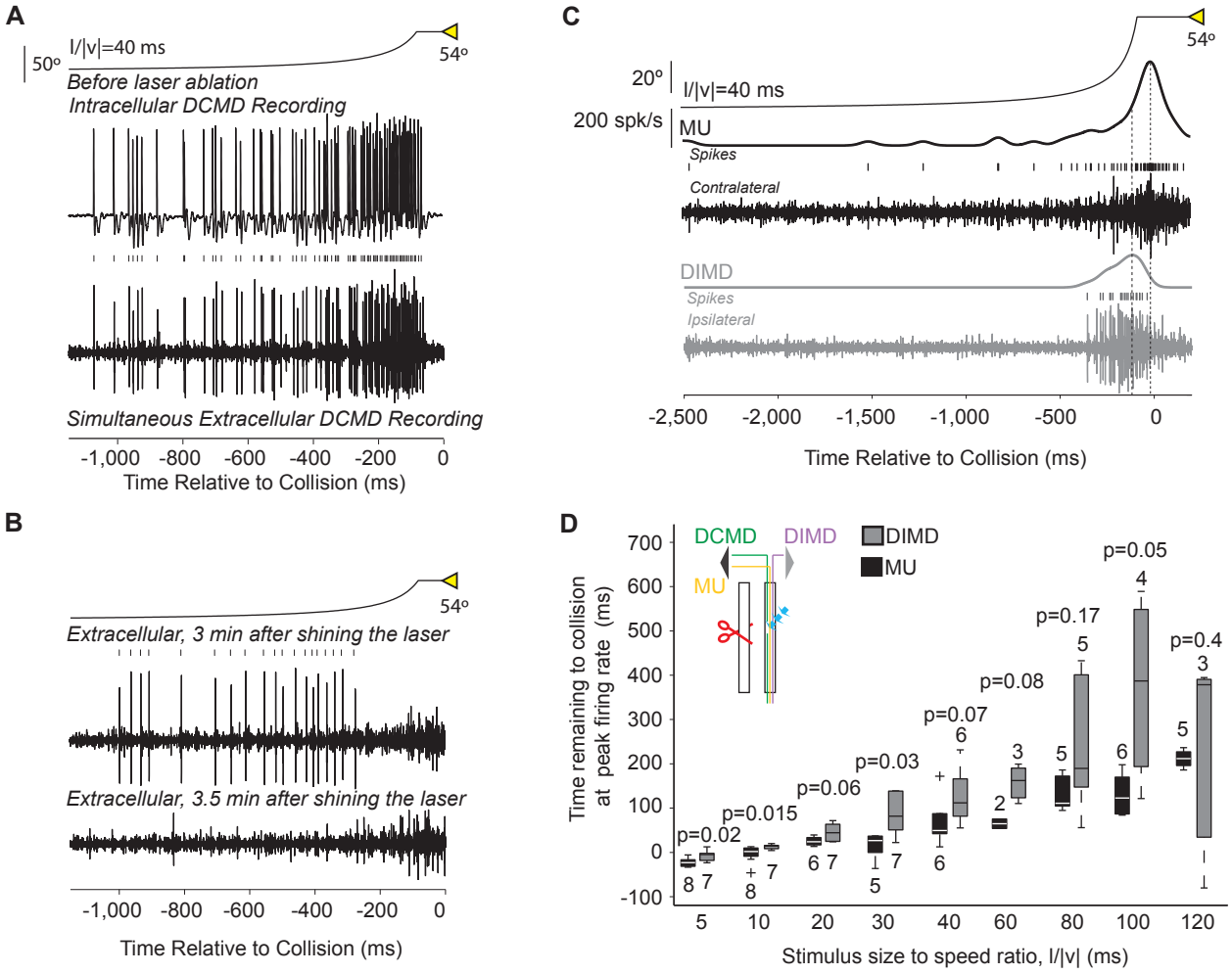

Figure- S7 (Fotowat et al.)